Magnetoluminescence characterization of lattice matched n-type InGaAs/InAlAs MQW's on InP

E. D. Jones[a], N. Kotera[b], T. Mishima[c], H. Nakamura[c], N. Miura[d], and C. P. Tigges[a]

a) Sandia National Laboratories, Albuquerque, NM 87185-0601, USA
b) Kyushu Institute of Technology, Iizuka, Fukuoka 820, Japan
c) Central Research Laboratory, Hitachi Ltd., Kokubunji, Tokyo 185, Japan.
d) Institute for Solid State Physics, University of Tokyo, Roppongi, Minato-ku, Tokyo 106, Japan

ABSTRACT

A knowledge of the energy-band energies and masses are important parameters for the design of semiconductor lasers and light-emitting diodes. We present results of a magnetoluminescence study on n-type ($N_{2D} \sim 1x10^{12}cm^{-2}$) InGaAs/InAlAs multiple quantum wells lattice matched to InP. From an analysis of low-temperature magnetoluminescence data, a simultaneous measurement of the in-plane conduction and valence-band masses is made. We find, assuming parabolic bands, that the conduction and valence-band masses are respectively $m_c \approx 0.069m_0$ and $m_v \approx 0.061m_0$, where m_0 is the free electron mass. Fitting a nonparabolic conduction-band dispersion curve to the data yields a zone-center mass $m_c \approx 0.056m_0$ and $m_v \sim 0.102m_0$.

Keywords: bandstructure, band masses, Landau levels, photoluminescence, magnetoluminescence

2. INTRODUCTION

The InAlGaAs material system is important for high speed optoelectronic devices. The most commonly used quantum well structures are nominally lattice matched to InP and with $In_{0.53}Ga_{0.47}As$ as the active layer and $In_{0.52}Al_{0.48}As$ as the barrier material. Typical room temperature bandgap wavelengths for InGaAs quantum wells are in the range about 1.3 to 1.6 μm, making this an attractive material system for high-speed low-loss fiber-optic based communication systems. In order to design state-of-the art quantum well structures for lasers, photodetectors, modulators, etc., several important band structure parameters such as bandgap energy E_g, conduction and valence band masses m_c and m_v and nonparabolic energy dispersion curve parameters are necessary for a successful design. While obtaining this kind of band structure detail for the strained layer InGaAs/GaAs system ($\lambda \approx 900$ nm) has been actively pursued,[1,2] there has not been the same level of experimental effort made for the 1.6 μm devices, presumably because of the lack of sensitive photodetectors for this wavelength regime when compared to standard photomultiplier tubes which operate in the wavelength range $\lambda \approx 300$nm to 1μm.

Bandgap energies and conduction-band masses for the InGaAs/InAlAs structures have been previously reported by several methods: (1) Studying the exciton absorption energy[3-8] and making corrections for the quasi two-dimensional (2D) exciton binding energy, which, because, of the valence-band offset, and conduction-band and valence-band mass uncertainties, is subject to error. In these absorption measurements, the conduction-band mass m_c varied from $0.041m_0$ (m_0 is the free electron mass) for an InGaAs/InP epilayer[3] and unintentionally doped InGaAs/InAlGaAs quantum (QW) structures to $0.053m_0$ for n-type InGaAs/InAlAs multi-quantum-well (MQW) structures.[8] (2) Photoconductivity measurements on heavily doped n-type InGaAs/InAlAs structures yielded conduction-band masses $m_c \approx 0.06m_0$.[9,10] The photoconductivity data were modeled in terms of estimates for the quantum confinement energies, i.e., valence-band offsets. (3) Magneto-Transport and optically detected cyclotron resonance measurements have been used to study band-edge masses $m_c \approx 0.043m_0$ for $In_x(Al_{1-y}Ga_y)_{1-x}As$/InP alloy epilayers[11] and for n-type InGaAs/InAlAs heterostructures,[12] $m_c \approx 0.044m_0$. (4) Recently,[13,14] cyclotron resonance studies reported on heavily doped InGaAs/InAlAs structures yielded even larger conduction band-masses $m_c \approx 0.06m_0$ which is attributed to nonparabolic conduction bands. For n-type 2D-systems, the conduction band masses are measured at the Fermi energy for both the cyclotron resonance and magneto-transport techniques. All of the aforementioned experimental methods, exciton absorption, cyclotron resonance, optically detected cyclotron resonance, and photoconductivity measurements have been mainly confined to n-type materials, while, except for one paper, [15] similar studies of valence-band masses from p-type InAlGaAs materials are practically nonexistent.

In this paper, we will present single-sample determinations for the all the above mentioned parameters using a recently perfected magnetoluminescence technique[16-20] and we will also make comparisons of previously reported results mentioned above. To demonstrate the utility of this technique, we report on magnetoluminescence measurement for an n-type multiquantum well InGaAs/InAlAs structure lattice matched to InP.

An accurate and unambiguous determination for the bandgap energy E_g also can be made from the magnetoluminescence transitions by extrapolating the magnetic field dependent Landau level transition energies to zero field. We will show that for heavily-doped n-type materials, the extrapolated bandgap energy E_g can differ by as much as 12 meV from the peak energy of the photoluminescence (PL) spectrum. Finally, the temperature dependence of the bandgap energy for n-type and undoped MQW structures will be compared.

3. EXPERIMENTAL

The magnetoluminescence measurements were made in the temperature range of 1.4 and 300 K, and the magnetic fields varied between 0 and 14 T. The sample was attached to the end of a 100 μm-core-diameter optical fiber and placed in a variable temperature insert in the middle of the superconducting magnet core. The luminescence measurements were made with an Argon-ion laser operating at 514.5 nm. The laser was injected into the optical fiber by means of a optical beam-splitter and the returning photoluminescence signal was directed to a 0.27M, f/4 optical monochromator with an IEEE-488 based data acquisition system. Typical laser power densities at the sample were less than 1 W/cm^2, therefore the photoinduced 2D-density of electrons and holes are very small, i.e., much less than 1×10^{10} cm^{-2}. A NORTH COAST EO-817 germanium detector was used to detect the infrared photons. The direction of the applied magnetic field is parallel to the growth direction, i.e., the resulting Landau orbits are in the plane of the quantum well. With this geometry, all measurements of the conduction and valence-band dispersion curves and masses are their *in-plane* values. The sample temperature was varied by a standard flowing low temperature He-gas system.

Two MQW structures, an n-type sample (#M5) and an undoped sample (#U10) were prepared using molecular beam epitaxy. The $In_{0.53}Ga_{0.47}As$ and $In_{0.52}Al_{0.48}As$ compositions were chosen to be lattice-matched to the Fe-doped, (100)-oriented InP substrates. The n-type InGaAs/InAlAs MQW structure was composed of ninety-nine pairs of a 5-nm-wide InGaAs quantum wells and a 10-nm-wide uniformly Si-doped (1×10^{18} cm^{-3}) InAlAs barrier. On top of these ninety-nine QW pairs, a single 10nm-wide InGaAs quantum well was also placed between two uniformly Si-doped InAlAs barriers. A schematic representation for the n-type MQW structure is shown in Fig.1.The undoped MQW structure consisted of ten pairs of 10nm-wide InGaAs quantum wells and 10nm-wide InAlAs barriers grown on top of a 1000-nm-thick undoped InAlAs buffer layer. A 300-nm-thick undoped InAlAs cap layer was then grown on top of the MQW layer. The growth temperatures were 440 and 500C respectively for the the n-type and undoped MQW structures. The growth rates for the InGaAs and InAlAs layers were about 1.1 to 1.2 μm/hour. For the n-type MQW sample, an intense PL signal near 930 meV was anticipated because of the large number (99) of 5nm-wide InGaAs QWs compared to the single 10 nm-wide InGaAs QW. Figure 2 shows the 1.5-K PL

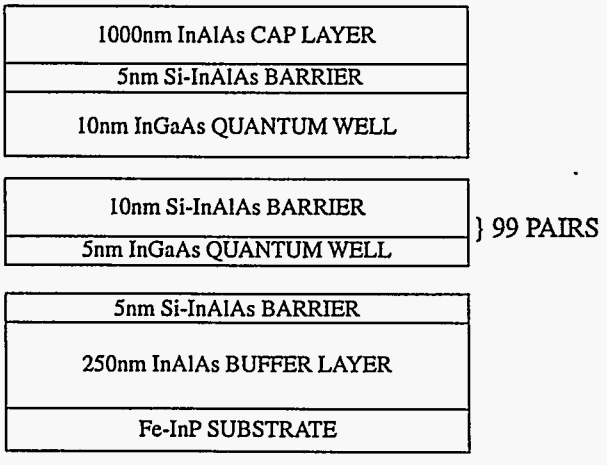

Figure 1. Structure of the n-type MQW consisting of ninety-nine pairs of 5nm-wide InGaAs/InAlAs QWs and a single 10nm-wide InGaAs/InAlAs QW.

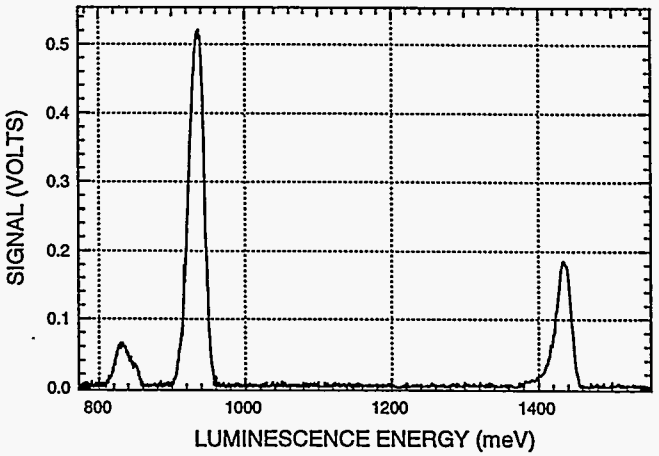

Figure 2. Low temperature (1.5K) PL spectrum for the n-type MQW. The peak at 1.43 eV is the InP substrate. The two PL peaks near 830 and 930 meV are respectively from the 10 and 5nm-wide InGaAs QWs.

spectrum for the n-type sample where the PL spectrum at 1.42 eV is the PL originating from the InP substrate material. The energy of the smaller intensity peak (left peak) is consistent with the PL energy from a heavily doped 10nm-wide InGaAs QW, and the intense peak near 930 meV (center peak) is the anticipated PL transition energy for the 5nm-wide InGaAs MQW structure. The 830 meV spectrum is found to shift linearly with magnetic field and also exhibits PL peaks associated with the formation of Landau levels. However, the 930 meV peak energy (and line shape) was found not to shift with applied magnetic fields, up to 13T, nor show the formation of Landau levels, suggesting that the origin for this transition should be assigned to strongly-bound extrinsic recombination processes such as donor-pair recombination, pinned excitons, interface states, etc., and not to band-to-band recombination between the heavily doped InGaAs QW conduction-band electrons and the photo-generated valence-band holes nor to recombination from free-excitons. Self-consistent Poisson equation calculations including quantum confinement, show, that depending upon empirical surface state densities, the ground state energy of a majority of the 5nm-wide quantum wells may be near or slightly above the structure's Fermi energy. With the apparent lack of magnetic field dependence to this PL transition energy and line shape, we conclude that this spectrum does not originate form intrinsic recombination processes and instead we will only report results for the single 10nm-wide QW.

4. BANDGAP ENERGIES AND MASSES

A charged particle, in the presence of a magnetic field B, forms a series of quantized states, Landau levels, with the quantized energy levels given by (cgs units) $\hbar\omega = (n + 1/2)(e\hbar B/mc)$, where $n = 0, 1, 2, \ldots$ is the Landau index, e is the charge of an electron, $\hbar$ is Planks' constant over 2π, m is the mass of the carrier, and c is the velocity of light. The distribution function for a degenerate two-dimensional electron gas (conduction-band states for a n-type material) is determined by the Fermi-Dirac statistics, but because of the very small number of photo-induced two-dimensional hole states, the distribution for the valence-band holes are governed by Maxwell-Boltzmann statistics. At high temperatures, where kT is much larger than $\hbar\omega$, the $n_v = 0, 1, 2, 3, \ldots$ valence-band Landau levels are populated and all magnetoluminescence transitions between the n_c and n_v Landau levels are *allowed,* obeying the $\delta n_{cv} \equiv (n_c - n_v) = 0$ selection rule. For these high temperatures, the interband luminescence transition energy E(n) is given by

$$E(n) = E_{gap} + \left(n + \frac{1}{2}\right)\left(\frac{e\hbar B}{\mu c}\right), \tag{1}$$

where E_{gap} is the bandgap energy, μ is the reduced mass ($\mu^{-1} = m_c^{-1} + m_v^{-1}$) where m_c and m_v are respectively the conduction and valence-band effective masses expressed in terms of the free electron mass m_0.

The conduction-band and valence-band energy levels (Landau levels) for the n-type structure in a magnetic field are shown in Fig. 3. The Fermi energy E_f, the bandgap energy E_g, and the Landau level indices are also indicated in the figure. For all discussions presented here, the Fermi energy E_f is always assumed to be large compared to kT. The high temperature case is shown on the right side of Fig. 3 where the population of the valence-band states is determined by Maxwell-Boltzmann statistics. For large magnetic fields and low temperatures, i.e., $kT << \hbar\omega_v$, only the $n_v = 0$ valence-band Landau level is populated. Here, the transition between the $n_c = 0$ and $n_v = 0$ Landau level is allowed, i.e., obeys the $\delta n_{cv} \equiv (n_c - n_v) = 0$ selection rule, while transitions between the higher energy conduction-band Landau levels $n_c = 1, 2, 3, \ldots$ and the $n_v = 0$ ground state valence-band Landau level are zeroth-order forbidden, but are observable.[21,22] due to higher order processes. The left side of Fig. 3 shows the energy level diagram for the low-temperature condition where only the $n_v = 0$ valence-band hole is occupied because the valence-band cyclotron energy is greater than the thermal energy kT.

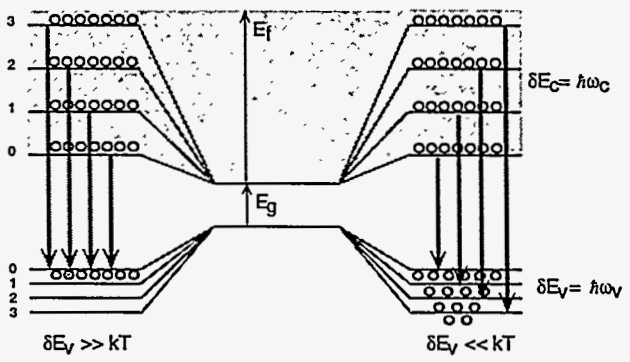

Figure 3. Landau levels for a n-type quantum well. The left side is the low temperature case, $\delta E_V \gg kT$, and the right side is the high temperature condition $\delta E_V \ll kT$.

As one can see from the left-hand side of Fig. 3, where $kT << \hbar\omega_v$, i.e. low temperatures, the energy difference $\delta E(n_c)$ between the $E(n_c)$ and $E(n_c\text{-}1)$ magnetoluminescence peaks depends only on $\hbar\omega_c$, the conduction-band cyclotron energy. Thus these zeroth-order forbidden transitions can be used to uniquely determine the conduction-band energy dispersion curves and/ or masses. Setting $n_v = 0$ and using Eq. 1, the magnetoluminescence transition energy difference $\delta E(n_c)$ is given by in terms of the respective conduction -band cyclotron energy (mass) as

$$\delta E(n_c) \equiv E(n_c) - E(n_c - 1) = \left(\frac{e\hbar B}{m_c c}\right), \tag{2}$$

where now $n_c = 1, 2, 3, \ldots$ Utilizing only low temperatures ($kT << \hbar\omega_v$) and measuring the energy differences of the zeroth-order forbidden transitions as a function of magnetic field, Eq. 2 gives the conduction-band mass while the slope of the allowed ($n_c = 0$) $\leftrightarrow$ ($n_v = 0$) transition energy as a function of magnetic field yields the reduced mass from Eq. 1. The valence-band mass m_v then can be calculated in terms of the conduction-band mass m_c and the measured reduced mass μ from ($m_v^{-1} = \mu^{-1} - m_c^{-1}$). The corrections to Eqs. 1 and 2 for nonparabolic bands have been reported in detail.[20]

The 1.4-K PL spectra for zero field and 8T are shown in Figs. 4 and 5 respectively. The signal gain of the data acquisition system for the zero-field spectrum (Fig. 4) is twice as large as that used for taking the 8-T spectrum (Fig. 5). The peak energy of the zero-field spectrum is about 832 meV and the change in slope near 855 meV, labeled E_f is due to transitions between the conduction electrons near the top of the Fermi-Dirac distribution and the valence-band holes. The bandgap energy E_g is indicated in the figure and a discussion for the determination will be presented below. Referring to Fig. 4, the difference between the bandgap energy E_g and the peak energy of the PL spectrum is the spectral shift (~12 meV) arising from carrier scattering by the ionized Si-dopants in the barriers as calculated by Lyo and Jones[23] and reported by Jones and Kurtz[24] for these kinds of systems.

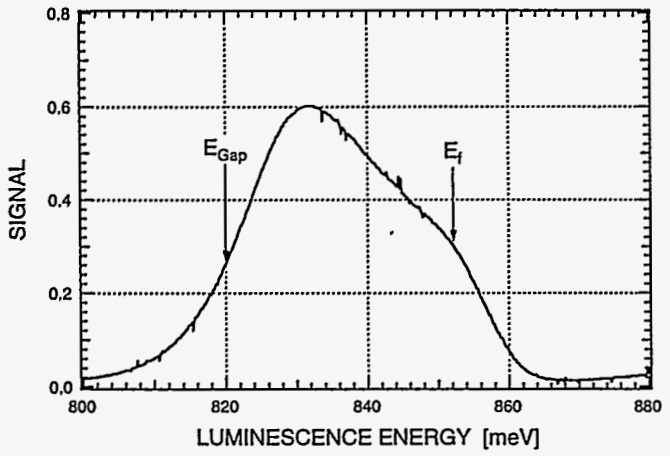

Figure 4. The zero-field, 1-4K PL spectrum for the n-type sample. The assignment for the bandgap energy E_g at 820 meV is discussed in the text.

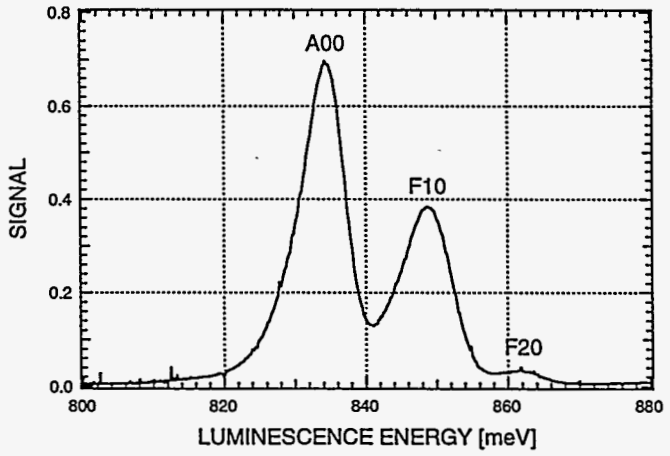

Figure 5. The 1-4K PL spectrum for the n-type sample at 8 tesla. The allowed transition peak is A00, and two zeroth-order forbidden transitions are labeled F10 and F20.

Three Landau level transitions are shown in Fig. 5 with an allowed ($n_c = 0$) $\leftrightarrow$ ($n_v = 0$) transition labeled A00 and two zeroth-order forbidden transitions ($n_c = 1$) $\leftrightarrow$ ($n_v = 0$) and ($n_c = 2$) $\leftrightarrow$ ($n_v = 0$) labeled respectively F10 and F20. A "fan" diagram for the all of the Landau level transition energies, allowed and forbidden, such as the three shown in Fig. 5 is shown in Fig. 6. The identification symbols for the allowed and various zeroth-order forbidden data are indicated in the inset in the figure. The straight lines drawn through the data shown in Fig 6, have a common zero-field intercept of 820 meV and is taken to be the bandgap energy $E_g$which is shown in Fig.4. The low-field data points are not considered in Fig. 4 because of spectral shifts of the zero-field spectrum discussed above. The use of a straight line fit to the data implies parabolic bands for both the conduction and valence-band dispersion curves. The ratio of slopes, normalized to the slope $\partial A00/\partial B = 1.755$ of the allowed-transition A00, are $\partial(F10)/\partial B = 1.93$, $\partial F20/\partial B = 3.22$, and $\partial F30/\partial B = 4.39$. If the zeroth-order forbidden transitions were incorrectly identified and all of the Landau level transitions were allowed, i.e., $\delta n_{cv} \equiv (n_c - n_v) = 0$, the slopes, with respect to the allowed-transition slope $\partial A00/\partial B$ would (see Eq. 1) be 3, 5, and 7.

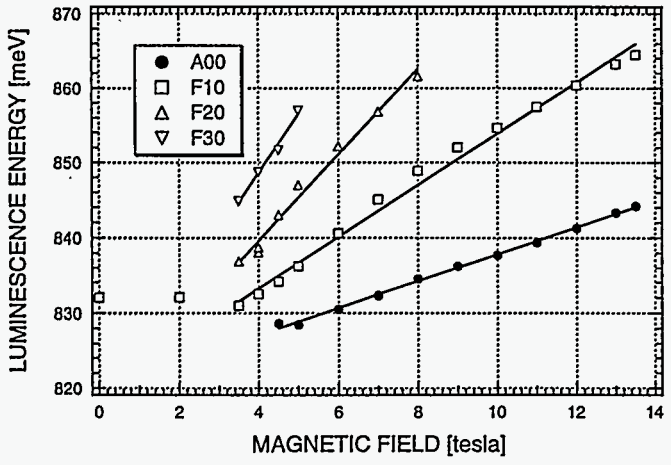

Figure 6. Fan diagram for the 1.4K magnetoluminescence spectrum for the n-type sample. The the assigned transition types are itemized in the inset.

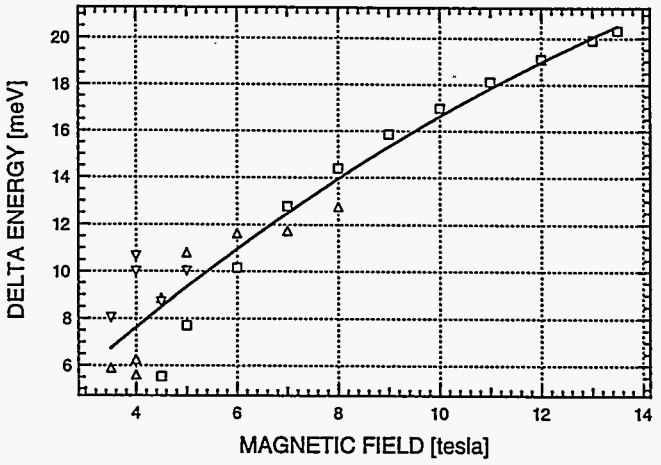

Figure 7. The energy difference $\delta E(n_c)$ as described by Eq. 2. The solid line is a least-squares fit of Eq. 3 to the data yielding a zone-center conduction-band mass $m_c = 0.56m_0$.

Figure 7 shows the energy difference $\delta E(n_c)$ as described by Eq. 2. The variation to the data at low fields results from our inability to accurately separate the closely spaced Landau-level peaks from each other in the PL spectrum. The conduction-band data can be analyzed in terms of parabolic or nonparabolic dispersion curves. The solid line drawn through the data is the nonparabolic case and is of the form

$$\delta E\left(n_c\right) = aB(1+bB), \tag{3}$$

where the fitting parameters a = 2.068 resulting in a zone center mass of $m_c = 0.056m_0$, and b = -1.963 x 10^{-2} is the nonparabolic contribution. From Fig.7, the conduction-band mass at the maximum field of 14T can be easily calculated to be $0.077m_0$ at the maximum magnetic field. A straight-line fit (i.e., parabolic bands) to the data shown in Fig 7 yields a conduction-band mass $m_c \approx 0.069m_0$.

As previously mentioned, with a knowledge of the conduction-band mass m_c, the reduced mass μ (Eq. 1) can be calculated from the slope $\partial A00/\partial B$ for the allowed $(n_c = 0) \leftrightarrow (n_v = 0)$ transition to be $\mu = 0.033m_0$, and from $(m_v^{-1} = \mu^{-1} - m_c^{-1})$, $m_v \approx 0.061m_0$ using the parabolic conduction-band mass of $0.069m_0$. If the conduction-band is nonparabolic as the curve drawn through the data of Fig. 7 suggests, then even if the valence-band was parabolic, the magnetic field dependence of the $(n_c = 0) \leftrightarrow (n_v = 0)$ transition shown in Fig 6 as A00, would have the same shape as the curve for the conduction-band data shown in Fig. 7. Because the allowed $(n_c = 0) \leftrightarrow (n_v = 0)$ transition (A00 in Fig. 6), is nearly linear, our data do not warrant a nonparabolic treatment for either the conduction or valence-band dispersion curves. Thus in this paper we will adopt the parabolic masses $m_c = 0.069m_0$ and $m_v = 0.061m_0$ for the conduction and valence-band masses respectively. Our magnetoluminescence determination for these masses yield results consistent with the previously reported masses for n-type InGaAs/InAlAs QWs.[7-15]

The zero-field 1.4-K PL spectrum for the 10nm-wide undoped InGaAs/InAlAs MQW sample is shown in Fig. 8. The peak energy is 857.5 meV and the FWHM is 6.0 meV. The bandgap energy for the undoped 10nm-wide InGaAs/InAlAs MQW sample is about 40 meV higher in energy than the 820 meV found above for the n-type 10nm-wide InGaAs/InAlAs MQW. There are several reasons for the lower bandgap energy of the n-type sample compared to the undoped sample. The reasons include bandgap reduction to spontaneous ordering (CuPt-type) which is known to lead to bandgap energy reductions. Another explanation are many-body effects, i.e., *bandgap renormalization*, due the large 2D-carrier density, and the last possibility may be attributable to InGaAs compositional differences. At the present time, we are not in a position to make any decision regarding these or any other possible explanations for the reduced bandgap energy. We are currently performing experiments and measurements which may shed light on this phenomena and the results and interpretations will be reported at a later date.

The magnetic field dependence between 0 and 14 tesla is shown in Fig. 9. The error estimates are given by ± (0.05 x FWHM). The FWHM is observed to decrease from 6.0 meV at 0T to 4.0 meV at 13.5T which suggests that the recombination is due to free excitons. The solid line drawn is a best-fit of the shift of a 2D-exciton in a magnetic field. This fitting procedure

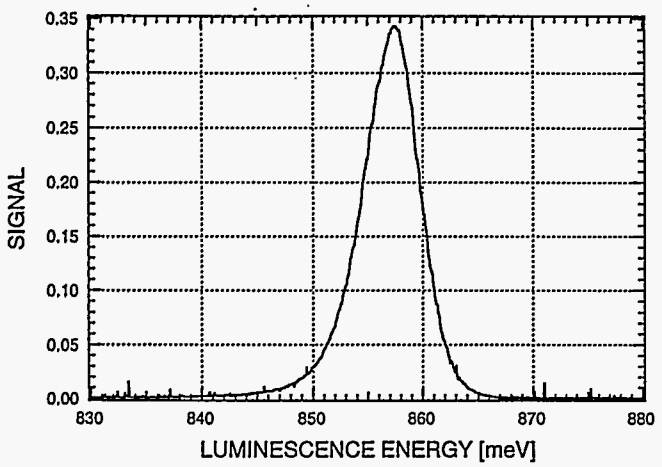

Figure 8. The PL spectrum at 1.4K for the undoped 10nm-wide InGaAs/InAlAs MQW. The peak of the spectrum is at 857.5 meV and the FWHM is 6.0 meV.

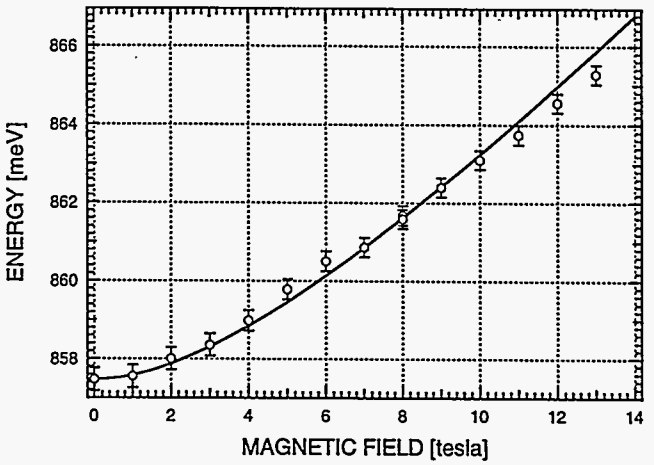

Figure 9. The magnetic field dependence of the exciton Pl spectrum peak energy at 1.4K for the undoped 10nm-wide InGaAs/InAlAs MQW. The error bar estimates are ± (0.05 x FWHM).

yielded an exciton reduced mass of $\mu = 0.041m_0$. An estimate for the conduction-band mass can be made if the valence-band mass is known, and vice-versa for an estimate for the valence-band mass. However, if we use the accepted value for *in-plane* zone-center conduction mass for undoped 10nm-wide quantum wells of $m_c \approx 0.041$, the the valence-band mass is heavy, $\sim 0.5m_0$. As is well known, the *in-plane* valence-band ground state masses of these QW systems are light and should be of the order of $0.050m_0$. On the other hand, the heavy-hole light-hole separation for a lattice-matched 10nm-wide QW is small, ~ 3 meV and our observed exciton energy shifts (Fig. 9) are large (~8 meV) indicating that the effects of magnetic field induced heavy-hole light-hole mixing should be properly accounted for when fitting exciton shift data.

5. TEMPERATURE DEPENDENCE OF THE BANDGAP ENERGY

The temperature dependence of the bandgap energy E_{gap} was measured between 1.4 and 300K for the undoped InGaAs/InAlAs structure and between 1.4 and 175K for the both t InGaAs/InAlAs samples. For temperatures larger than 175K the PL signal-to-noise ratio for the n-type MQW structure was too small to make meaningful interpretations and also, the linewidth was too broad to be able to observe any Landau levels in the noisy PL spectrum. The bandgap energy for the n-type sample was estimated by performing magnetoluminescence measurements at each temperature and extrapolating each "fan" diagram (see Fig. 6) to zero field. The bandgap energy for the undoped sample is taken as the peak of the exciton PL spectrum as shown in Fig. 8. The true bandgap energy would include the exciton binding energy. Because here we are only interested in comparing the temperature dependence between the n-type and undoped samples, we have not taken this binding energy into account. The solid lines drawn through the data are based on the Varshni equation[25] for the temperature dependence of the bandgap energy, e.g., $E(T) = E_{gap} + \alpha T^2/(T + ß)$, where E_{gap}, α, and ß are fitting parameters. For the undoped MQW structure, the best fit parameters are E_{gap} = 860 meV, $\alpha = 1.29$ meV/K^2, ß = 1440 meV/K. For the n-type samples the same parameters are E_{gap} = 822 meV, $\alpha = 0.52$ meV/K^2, ß = 343 meV/K. For both structures, the bandgap energies which are extracted from the temperature dependent data, are close to those found at 1.4K. The two other fitting parameters α and ß are for reference only and provide the numerics necessary for calculating the bandgap energy at a given temperature.

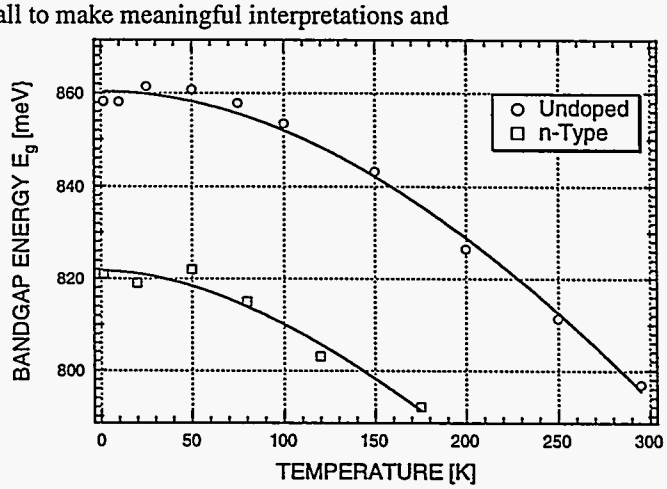

Figure 10. Temperature dependencies of the bandgap energies for the n-type and undoped InGaAs/InAlAs MQW.

6. SUMMARY

In this paper, we have presented a measurement of the conduction-band mass for an n-type InGaAs/InAlAs MQW using low-temperature magnetoluminescence techniques. As was the case with other experimental techniques, we measure a conduction-band mass $m_c \approx 0.069m_0$ which is also considerably heavier than the accepted $m_c \approx 0.041m_0$ band-edge mass. Because the n-type sample structure did not show any meaningful luminescence from the 5nm-wide-well portion of the sample, we are currently redesigning these kinds of structures using a self-consistent Poisson's calculation including quantum confinement for the bandstructure to provide guidance. Data for an undoped 10nm-wide InGaAs/InAlAs MQW structure was taken as a function of magnetic field and temperature and when possible, comparisons with similar n-type data were made.

7. ACKNOWLEDGMENTS

The authors wish to thank Dr. Kyu-Seok Lee for performing the magnetoexciton fitting routines, and Dr. M. H. Crawford for critical reading of the manuscript. This work was supported in part by the Division of Material Science, Office of Basic Energy Science, U. S. DOE, No. DE-AC04-94AL8500.

8. REFERENCES

1. G. C. Osbourn, P. L. Gourley, I. J. Fritz, R. M. Biefeld, L. R. Dawson, and T. E. Zipperian, "Principals and Applications of Semiconductor Strained-Layer Superlattices," in *Semiconductors and Semimetals,* Edited by R. Dingle, Vol. 24, page 459, Academic Press, NY, 1987.
2. T. P. Pearsall, "Strained-Layer Superlattices," in *Semiconductors and Semimetals*, Edited by T. P. Pearsall, Vol. 32, page 1, Academic Press, NY, 1990.
3. K. Alavi and R. L. Aggarwal, "Interband magnetoabsorption of $In_{0.53}Ga_{0.47}As$, Phys. Rev. **B21**, 1311 (1980).
4. D. C. Rogers, R. J. Nicholas, S. Ben Amor, J. C. Portal, A. Y. Cho, and D. Sivco, "Inter-band magneto-absorption in $Ga_{0.47}In_{0.53}As$-$Al_{0.48}In_{0.52}As$ quantum well", Solid State Commun. **60**, 83 (1986).
5. W. Stolz, J. C. Maan, M. Altarelli, L. Tapfer, and K. Ploog, "Absorption spectroscopy on $Ga_{0.47}In_{0.53}As/Al_{0.48}In_{0.52}As$ multi-quantum-well heterostructures I. Excitonic transitions", Phys. Rev. **B36**, 4301 (1987).
6. W. Stolz, J. C. Maan, M. Altarelli, L. Tapfer, and K. Ploog, "Absorption spectroscopy on $Ga_{0.47}In_{0.53}As/Al_{0.48}In_{0.52}As$ multi-quantum-well heterostructures II. Subband structure", Phys. Rev. **B36**, 4310 (1987).
7. T. W. Kim, M. Jung, D. U. Lee, K-H Yoo, and K-H Yoo, "Magnetotransport, magneto-optical, and electronic subband studies in $In_xGa_{1-x}As/In_{0.52}Al_{0.48}As$ one-side-modulation-doped asymmetric set quantum wells", Appl. Phys. Lett. **69**, 1752 (1996).
8. T. W. Kim, M. Jung, D. U. Lee, K-H Yoo, and K-H Yoo, "Magnetotransport, magneto-optical, and electronic subband studies in highly strained $In_xGa_{1-x}As$/InP one-side-modulation-doped double quantum wells", Semi. Sci. Technol. **11**, 84 (1996)
9. N. Kotera and K. Tanaka, "Photocurrent spectroscopy of 2-dimensional excitons in 5-nm-wide InGaAs/InAlAs multi quantum wells, *Inst. Phys. Conf. Ser.* No **141**, 233 (1994).
10. N. Kotera, K. Tanaka, and H. Nakamura, "Photocurrent spectroscopy of 5-nm-wide InGaAs/InAlAs quantum wells and quadratic dependence of optical transition energies on quantum numbers," *J. Appl. Phys.* **78**, 5168 (1995).
11. Y. F. Chen, Y. T. Dai, J. C. Fan, T. L. Lee, and H. H. Lin "Dependence of electron effective mass on alloy composition of InAlGaAs lattice matched to InP studied by optically detected cyclotron resonance," *Appl. Phys. Lett.* **67**, 1256 (1995).
12. Y. F. Chen, Y. T. Dai, and I. Lo, "Observation of double cyclotron resonance in modulation-δ-doped $In_{0.52}Al_{0.48}A$/ $In_{0.53}Ga_{0.47}As$" *Appl. Phys. Lett.* **68**, 1117 (1996).
13. N. Kotera, Y. Shimamoto, T. Mishima, and N. Miura, "Study of cyclotron resonance in very high magnetic fields and non-parabolic energy band in InGaAs/InAlAs quantum wells," *Physica B* **227**, 349 (1996).
14. N. Kotera, Y. Shimamoto, H. Arimoto, N. Miura, and T. Mishima, "Electron effective mass in nanoscale InGaAs/InAlAs multi-quantum wells determined by cyclotron resonance in intense magnetic fields," *(to be published)*
15. C. Hermann and T. P. Pearsall, "Optical pumping and the valence-band light-hole effective mass in $Ga_xIn_{1-x}As_yP_{1-y}$ ($y \approx 2.2x$)", Appl. Phys. Lett. **38**, 450 (1981).
16. E. D. Jones, S. K. Lyo, I. J. Fritz, J. F. Klem, J. E. Schirber, C. P. Tigges, and T. J. Drummond, "Determination of energy-band dispersion curves for strained-layer structures," *Appl. Phys. Lett.* **54**, 2227 (1989).
17. E. D. Jones, R. M. Biefeld, J. F. Klem, and S. K. Lyo, "Strain and density dependent valence-band masses in InGaAs/ GaAs and GaAs/GaAsP strained-layer structures," *Proceedings. 16th International Symposium on GaAs and Related materials*, Karuizawa, Japan 1989, *Inst. Phys. Conf. Ser.* No. 106, 435 (1990).

18. E. D. Jones, L. R. Dawson, J. F. Klem, S. K. Lyo, D. Heiman, and X. C. Liu, "Magnetic-field dependent photoluminescence studies of InGaAs/GaAs strained-single-quantum wells", *The Applications of High Magnetic Fields in Semiconductor Physics (SEMIMAG-94)*, Edited by D. Heiman (World Scientific Publishing, 1995) pp. 332 - 335.
19. E. D. Jones, L. R. Dawson, J. F. Klem, S. K. Lyo, D. Heiman, and X. C. Liu, "Optical Determination of conduction and valence-band dispersion curves in strained-single-quantum wells", *Proceedings 22nd Inter. Conf. Phys. of Semiconductors, Vancouver, Canada*, Edited by D. J. Lockwood, pp. 1492-1494 (World Scientific Publishing, Singapore, 1995)
20. E. D. Jones, S. K. Lyo, and J. F. Klem, "Determination of band structure dispersion curves by optical techniques, *Proceedings, 22nd International Symposium on Compound Semiconductors*, Cheju Island, Korea, August 28 - September 2, 1995, *Inst. Phys Conf. Ser. No* **145**, 397 (1996).
21. S. K. Lyo, E. D. Jones, and J. F. Klem, "Breaking of the usual selection rule for magnetoluminescence in doped semiconductor quantum-wells," *Phys. Rev. Lett.* **61**, 2265 (1988).
22. S. K. Lyo, "Theory of optical spectra in a magnetic field in doped semiconductor quantum wells: Impurity-induced broadening and transitions," *Phys. Rev. B* **40**, 8418 (1989).
23. S. K. Lyo and E. D. Jones, "Photoluminescence line shape in degenerate semiconductor quantum-wells", Phys. Rev. B **38**, 4113 (1988).
24. E. D. Jones and S. R. Kurtz, Magnetoluminescence characterization of quantum well structures, in Semiconductor Characterization: Present Status and Future Needs, Edited by W. M. Bullis, D. G. Deiler, and A. C. Diebold (Am. Inst. Phys. Woodbury, NY 1996), pp. 591 - 598
25. Y. P. Varshni, "Temperature dependence of the energy gap in semiconductors", Physica **34**, 149 (1967).

DISCLAIMER